INTERNATIONAL JOURNAL FOR NUMERICAL METHODS IN ENGINEERING
Int. J. Numer. Meth. Engng 2010; **83**:851–876
Published online 9 March 2010 in Wiley InterScience (www.interscience.wiley.com). DOI: 10.1002/nme.2860

Subdomain radial basis collocation method for fracture mechanics

Lihua Wang[1], Jiun-Shyan Chen[2,*,†,‡] and Hsin-Yun Hu[3,§]

[1]*School of Aerospace Engineering and Applied Mechanics, Tongji University, Shanghai, People's Republic of China*
[2]*Civil and Environmental Engineering Department, University of California Los Angeles (UCLA), Los Angeles, CA 90095, U.S.A.*
[3]*Mathematics Department, Tunghai University, Taichung 407, Taiwan*

SUMMARY

The direct approximation of strong form using radial basis functions (RBFs), commonly called the radial basis collocation method (RBCM), has been recognized as an effective means for solving boundary value problems. Nevertheless, the non-compactness of the RBFs precludes its application to problems with local features, such as fracture problems, among others. This work attempts to apply RBCM to fracture mechanics by introducing a domain decomposition technique with proper interface conditions. The proposed method allows (1) natural representation of discontinuity across the crack surfaces and (2) enrichment of crack-tip solution in a local subdomain. With the proper domain decomposition and interface conditions, exponential convergence rate can be achieved while keeping the discrete system well-conditioned. The analytical prediction and numerical results demonstrate that an optimal dimension of the near-tip subdomain exists. The effectiveness of the proposed method is justified by the mathematical analysis and demonstrated by the numerical examples. Copyright © 2010 John Wiley & Sons, Ltd.

Received 15 September 2009; Revised 6 January 2010; Accepted 8 January 2010

KEY WORDS: radial basis collocation method; subdomain partitioning; fracture mechanics; crack problems; radial basis function

1. INTRODUCTION

Radial basis functions (RBFs) have been widely used in reconstruction of functions from known data [1–4] and as the basis functions for solving partial differential equations (PDEs) [5–10].

*Correspondence to: Jiun-Shyan Chen, Civil and Environmental Engineering Department, University of California Los Angeles, Los Angeles, CA 90095, U.S.A.
†E-mail: jschen@seas.ucla.edu
‡Professor.
§Assistant Professor.

Contract/grant sponsor: National Natural Science Foundation of China (NSFC); contract/grant number: 10572104
Contract/grant sponsor: US Army ERDC; contract/grant number W912HZ-07-C-0019
Contract/grant sponsor: National Science Council of Taiwan; contract/grant number NSC 96-2115-M-029-002-MY2

The mathematical theories for convergence in the RBF approximation can be found in [11–15]. Despite of its progress in recent years, difficulties remain when a large number of RBFs are used in the approximation and when local features exist. These difficulties are largely attributed to the non-compactness of the RBFs.

One typical example of problems with local features is the one with heterogeneity in the coefficients of PDEs, such as elasticity with heterogeneous materials. The local characters in this type of problems cannot be precisely represented by the nonlocal RBFs. Further, derivative discontinuities across the material interfaces cannot be properly approximated by RBFs. Several attempts have been introduced to localize the RBFs. These methods include a class of positive definite and compactly supported radial functions which consist of a univariate polynomial within their support [16, 17], a local weighted residual method with the Heaviside step function as the weighting function over a local domain and with the RBF as the trial function [18], introducing an influence domain to the RBF approximation where each influence domain is localized [19], introducing RBF in the direct collocation of PDE by computing derivatives based on a differential quadrature scheme within a local domain of influence [20], and a reproducing kernel-enhanced RBF approximation to achieve a local approximation while possessing a similar convergence property as that of the nonlocal RBF [21]. The issue of treating derivative discontinuity when using smooth approximation functions has been addressed largely in the Galerkin-type methods, such as the element free Galerkin (EFG) or reproducing kernel particle method (RKPM), by introducing Lagrange multiplier method [22] and interface enrichment techniques [23]. In the strong form type method such as radial basis collocation method (RBCM), a subdomain collocation method [24] has been proposed, where RBF approximation in each subdomain is constructed separately, and compatibility and flux equilibrium conditions are then imposed on the interfaces between subdomains. This approach yields a derivative discontinuity on the interface and retains an exponential convergence of RBCM when solving problems with heterogeneity.

Fracture mechanics represents another class of problems that are difficult to be solved by numerical methods using smooth approximation functions. The roughness of the solution in fracture problems includes strong discontinuity across fracture surfaces and singularities in the stress field at the crack tip. Galerkin methods with smooth approximation typically yield a rather slow convergence in fracture problems [25]. The non-convex geometry of crack surface adds additional complexity in methods where approximation functions are not constructed from the local mesh. Belytschko and co-authors introduced a method [26] to modify the moving least-squares (MLS) approximation functions near the crack tip to yield a discontinuity in the approximation functions across the crack surfaces. To further enhance the solution accuracy near crack tip where stress singularity exists, enrichment functions representing crack-tip characteristics were introduced to nodes near the crack tip as extrinsic bases [27, 28] or as intrinsic bases [27] of MLS. Other meshfree methods have also been proposed for fracture problems, such as extended finite element method [29, 30], collocation Trefftz method [31] and point collocation method [32].

Most of the above-mentioned methods for computational fracture mechanics are of weak form type. In this work, we focus on the methods based on strong form approach, specifically, under the framework of the RBCM. Employing RBCM for solving Motz's problem where singularity exists on the boundary has been introduced by Hu *et al.* [9]. Owing to the singularity at the source points, singular functions were introduced in the RBF approximation to solve Motz's problem. In the present work, we first introduce domain decomposition under the framework of subdomain collocation method to deal with the discontinuity across the crack surface. The domain is separated into three subdomains: a small circular domain near the crack tip and two larger subdomains

DOI: 10.1002/nme

separated by the extension of the crack surface. The approximation in each subdomain is constructed separately, and compatibility and traction equilibrium conditions are then imposed on the interfaces between subdomains. Enrichment functions with $\sqrt{r}$ property and discontinuity cross crack surface are introduced in the near-tip subdomain, while multiquadrics RBFs are employed for the other subdomains away from the crack tip. Selection of proper dimension for the near-tip subdomain can be estimated by keeping the balance of errors among the subdomain interfaces near the crack tip.

The remainder of this paper is organized as follows. The overview of RBF approximations and the convergence properties are given in Section 2. In Section 3, we first demonstrate that the enriched RBCM with the visibility criteria (RBCM-VC) or the diffraction method introduced in EFG [26–29] yields unsatisfactory results. Further, adding crack-tip enrichment functions to the RBF approximation results in an ill-conditioned discrete system. The subdomain radial basis collocation method (SD-RBCM) is also reviewed in this section. In Section 3, enriched SD-RBCM for fracture mechanics is introduced. The strategy of domain decomposition for introducing different basis functions in different subdomains is presented, proper interface conditions between subdomains are introduced, and discretization by strong form collocation for fracture problems is derived. The error analysis of the proposed method is given in this section as well. The effectiveness of the proposed method is demonstrated in the numerical examples presented in Section 4. Finally, concluding remarks are given in Section 5.

2. RADIAL BASIS COLLOCATION METHOD

Boundary value problems have traditionally been solved by the Galerkin method, where the original strong formulation is first transformed to a weak formulation. Weak formulation has also been employed in meshfree methods where the approximation functions are constructed without using local element topology, and thus the constraint on element boundary compatibility is avoided. Nevertheless, the need to integrate domain in the weak formulation adds considerable complexity to meshfree methods. An alternative approach for solving PDEs is to introduce approximation directly to the strong form. The strong form approach appears to be attractive for meshfree methods as it avoids domain and boundary integrations. The higher-order differentiability of many RBFs makes them good candidates for solving PDEs using the strong formulation with collocation [5, 8], termed the RBCM as described below.

2.1. RBCM for boundary value problems

Consider the following boundary value problem:

$$\mathbf{L}\mathbf{u} = \mathbf{f} \quad \text{in } \Omega \tag{1}$$

$$\mathbf{B}_g\mathbf{u} = \mathbf{g} \quad \text{on } \partial\Omega_g \tag{2}$$

$$\mathbf{B}_h\mathbf{u} = \mathbf{h} \quad \text{on } \partial\Omega_h \tag{3}$$

where $\mathbf{L}$ is the differential operator, $\mathbf{B}_g$ and $\mathbf{B}_h$ are the boundary operators associated with Dirichlet and Neumann boundary conditions, respectively, Ω is the problem domain, $\partial\Omega_g$ is the Dirichlet boundary, $\partial\Omega_h$ is the Neumann boundary, $\mathbf{f}$, $\mathbf{g}$, $\mathbf{h}$ are the source term tensors, and $\mathbf{u}$ is the unknown tensorial function.

DOI: 10.1002/nme

Equations (1)–(3) are called the strong forms of the boundary value problem in which the solution $\mathbf{u}$ is approximated by some basis functions. The approximated function $\mathbf{v} \approx \mathbf{u}$ is forced to satisfy the strong forms (1)–(3) at the collocation points:

$$\mathbf{L}\mathbf{v}(\mathbf{p}_I) = \mathbf{f}(\mathbf{p}_I), \quad \mathbf{p}_I \in \Omega, \quad I = 1, \ldots, N_p \tag{4}$$

$$\mathbf{B}_g\mathbf{v}(\mathbf{q}_I) = \mathbf{g}(\mathbf{q}_I), \quad \mathbf{q}_I \in \partial\Omega_g, \quad I = 1, \ldots, N_q \tag{5}$$

$$\mathbf{B}_h\mathbf{v}(\mathbf{r}_I) = \mathbf{h}(\mathbf{r}_I), \quad \mathbf{r}_I \in \partial\Omega_h, \quad I = 1, \ldots, N_r \tag{6}$$

where $\{\mathbf{p}_I\}_{I=1}^{N_p} \subseteq \Omega$, $\{\mathbf{q}_I\}_{I=1}^{N_q} \subseteq \partial\Omega_g$, and $\{\mathbf{r}_I\}_{I=1}^{N_r} \subseteq \partial\Omega_h$ are the collocation points in domain Ω, and on the Dirichlet boundary $\partial\Omega_g$ and the Neumann boundary $\partial\Omega_h$, respectively. Let the approximated function be expressed as

$$\mathbf{v}(\mathbf{x}) = \sum_{I=1}^{N_s} \phi_I(\mathbf{x})\mathbf{a}_I = \mathbf{\Phi}^{\mathrm{T}}\mathbf{a} \tag{7}$$

where $\mathbf{v}^{\mathrm{T}} = [v_1, v_2, v_3]$, $\mathbf{a}^{\mathrm{T}} = [\mathbf{a}_1, \ldots, \mathbf{a}_{N_s}]$, $\mathbf{a}_I^{\mathrm{T}} = [a_{1I}, a_{2I}, a_{3I}]$, $\mathbf{\Phi}^{\mathrm{T}} = [\mathbf{\Phi}_1, \ldots, \mathbf{\Phi}_{N_s}]$, $\mathbf{\Phi}_I = \phi_I\mathbf{I}$, ϕ_I is the basis function centered at source point $\mathbf{x}_I$, and N_s is the number of source points. Introducing approximation (7) into the collocation equations (4)–(6), we have

$$\mathbf{L}\mathbf{\Phi}^{\mathrm{T}}(\mathbf{p}_I)\mathbf{a} = \mathbf{f}(\mathbf{p}_I), \quad \mathbf{p}_I \in \Omega, \quad I = 1, \ldots, N_p \tag{8}$$

$$\mathbf{B}_g\mathbf{\Phi}^{\mathrm{T}}(\mathbf{q}_I)\mathbf{a} = \mathbf{g}(\mathbf{q}_I), \quad \mathbf{q}_I \in \partial\Omega_g, \quad I = 1, \ldots, N_q \tag{9}$$

$$\mathbf{B}_h\mathbf{\Phi}^{\mathrm{T}}(\mathbf{r}_I)\mathbf{a} = \mathbf{h}(\mathbf{r}_I), \quad \mathbf{r}_I \in \partial\Omega_h, \quad I = 1, \ldots, N_r \tag{10}$$

Equations (8)–(10) are combined to solve for the coefficient vector $\mathbf{a}$:

$$\underbrace{\begin{bmatrix} \mathbf{A}_L \\ \mathbf{A}_g \\ \mathbf{A}_h \end{bmatrix}}_{\mathbf{A}} \mathbf{a} = \underbrace{\begin{bmatrix} \mathbf{b}_L \\ \mathbf{b}_g \\ \mathbf{b}_h \end{bmatrix}}_{\mathbf{b}} \tag{11}$$

where the sub-matrices in (11) are given in Appendix A. For achieving sufficient accuracy in using RBF approximation for the numerical solution of PDEs, the total number of collocation points $N_c = N_p + N_g + N_r$ much larger than the number of source points N_s should be used [33]. This yields an over determined system in (11), and approaches such as least-squares method is used to obtained an approximate solution.

The convergence of the discrete equation (11) is closely related to the basis functions used in the approximation (7). The required continuity of the basis functions is determined by the differential operator $\mathbf{L}$. Without integration by parts commonly used in the weak formulation, basis functions with higher-order continuity are needed in this strong form-based approach compared with the Galerkin method. The most commonly used basis function for the strong form collocation method is the multivariate RBFs originally constructed for surface fitting [1]. Some RBFs perform very well in interpolating highly irregular scattered data compared with many interpolation methods [2], and they have been introduced in high-dimensional interpolation [34]. RBF was first applied

DOI: 10.1002/nme

to solving PDEs in [5, 6]. A commonly used RBF for solving PDEs is the multiquadratics (MQ) function [1, 12]:

$$\phi_I(\mathbf{x}) = (r_I^2 + c^2)^{n-3/2}, \quad n = 1, 2, 3, \ldots \tag{12}$$

where $r_I = \|\mathbf{x} - \mathbf{x}_I\|$, and the constant c is called the shape parameter of RBF. To reproduce certain order of polynomials, the approximation by RBF is often modified as

$$v_i(\mathbf{x}) = \sum_{I=1}^{N_s} \phi_I(\mathbf{x}) a_{iI} + p(\mathbf{x}) \tag{13}$$

where $p(\mathbf{x}) \in \mathbf{P}_m$ is complete polynomials of degree less and equal to m. The convergence of RBF has been studied by Madych and Nelson [11], and it has been shown that there exists an exponential convergence rate if RBF is globally analytic or band-limited

$$\|\mathbf{u} - \mathbf{v}\|_{L^\infty(\Omega)} \leqslant C\eta^{c/h} \|\mathbf{u}\|_t \tag{14}$$

where C is a constant independent of c and h, h is the radial distance between source points, $0 < \eta < 1$ is a real number, and $\|\cdot\|_t$ is induced form defined in [11].

RBFs such as MQ function in (12) are nonlocal functions. This yields a full matrix $\mathbf{A}$ in (11) and consequently ill-conditioned as the dimension of $\mathbf{A}$ increases. Following [21], the condition number of $\mathbf{A}$ is given as

$$\mathrm{Cond}(\mathbf{A}) = \frac{\sigma_{\max}(\mathbf{A})}{\sigma_{\min}(\mathbf{A})} = \left(\frac{\lambda_{\max}(\mathbf{A}^{\mathrm{T}}\mathbf{A})}{\lambda_{\min}(\mathbf{A}^{\mathrm{T}}\mathbf{A})} \right)^{1/2} \approx O(N_S^4) \tag{15}$$

where $\lambda_{\min}(\mathbf{A}^{\mathrm{T}}\mathbf{A})$ and $\lambda_{\max}(\mathbf{A}^{\mathrm{T}}\mathbf{A})$ are the minimal and maximal eigenvalues of matrix $\mathbf{A}^{\mathrm{T}}\mathbf{A}$, respectively. As shown in (15), the condition number increases quickly in the model refinement, which is needed in problems with local features such as heterogeneity and singularity. A subdomain collocation method [24] has been introduced to reduce the condition numbers and to model heterogeneous media where derivative discontinuity exists. This idea will be extended to fracture mechanics in this work where singularity in stresses and strains requires special treatment using RBF approximation.

2.2. *Difficulty in RBCM for fracture mechanics*

Meshfree methods with smooth and node-based approximation encounter difficulties in approximating strong discontinuity (C^{-1}) across crack surface and singularity in strain and stress fields at the crack tip. A commonly used approach under the Galerkin framework is to introduce enrichment functions in the approximation as [27]

$$\mathbf{v}(\mathbf{x}) = \tilde{\mathbf{v}}(\mathbf{x}) + \hat{\mathbf{v}}(\mathbf{x}) \tag{16}$$

where $\tilde{\mathbf{v}} \in C^n$ is a smooth function with continuity $n \geqslant 0$, and $\hat{v}$ is the enrichment function expressed as follows for the near-tip field:

$$\hat{\mathbf{v}}(\mathbf{x}) = \sum_{I=1}^{4} \hat{\phi}_I(\mathbf{x}) \hat{\mathbf{a}}_I = \hat{\mathbf{\Phi}}^{\mathrm{T}} \hat{\mathbf{a}} \tag{17}$$

DOI: 10.1002/nme

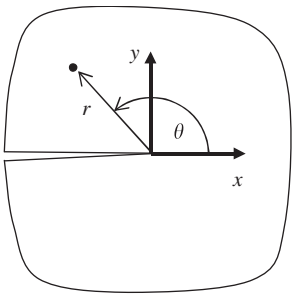

Figure 1. Crack surface geometry and orientation.

where

$$\hat{\mathbf{\Phi}}^{\mathrm{T}} = \left[\sqrt{r}\sin\frac{\theta}{2}, \sqrt{r}\cos\frac{\theta}{2}, \sqrt{r}\sin\frac{\theta}{2}\sin\theta, \sqrt{r}\cos\frac{\theta}{2}\sin\theta \right] \tag{18}$$

Here θ is the angle tangent to the crack surface as shown in Figure 1. The bases $\hat{\phi}_I$ for the enrichment function $\hat{\mathbf{v}}$ are selected based on the asymptotic displacement field near crack tip, and they exhibit strong discontinuity along $\theta \to \pi$ and $\theta \to -\pi$. The term $\sqrt{r}$ is the asymptotic displacement behavior which yields $1/\sqrt{r}$ singularity in strain and stress fields near the crack tip. Although the enrichment function $\hat{\mathbf{v}}$ constructed above enhances solution accuracy near the crack tip, the convergence of the total solution resides on the basis functions in the smooth part $\tilde{\mathbf{v}}$.

Under the framework of element free Galerkin [28], MLS functions have been employed as the bases for $\tilde{\mathbf{v}}$. A visibility criterion has been proposed in the construction of $\hat{\phi}_I$ where the domain of influence of the MLS functions is truncated according to the crack surface intersecting with the ray of light between the nodal point and point of evaluation. This approach, however, introduces discontinuity along certain direction inside the problem domain and the method yields incorrect stress and strain fields and performs poorly when crack-tip enrichment functions are introduced [27]. A transparency method and a diffraction method have been introduced to yield MLS functions with only discontinuity across the crack surface and maintain proper continuity inside the domain [26]. However, we observe that the above methods do not work well for strong form collocation with radial basis approximation functions as demonstrated below.

To demonstrate, a plane stress plate with an edge crack subjected to a uniform tension $\sigma = 1.0$ is considered (Figure 2(a)). The plate dimension is 0.6×0.6, and the crack length is 0.3. The material properties of the plate are Young's modulus $E = 3 \times 10^4$ and the Poisson ratio $v = 0.3$. This problem is solved by a strong form collocation in (8)–(11) using MQ RBF in (12) with $n = 1$ for the smooth approximation $\tilde{\mathbf{v}}$. Bases in (18) are used as the near-tip enrichment functions for $\hat{\mathbf{v}}$. We also weight the boundary conditions in (9) and (10) according to [10]. The number of collocation points is four times of the number of source points for this problem as shown in Figure 2(b). Since RBFs are not compactly supported, we use visibility criterion to introduce discontinuity in the RBFs as shown in Figure 2(c). The RBF domain of influence for source point P in a cracked square domain is truncated by the line connecting the source point P and the crack tip Q using the visibility criterion. The truncated RBF associated with the source point P becomes discontinuous across crack surface and across line $\overline{QP}$. We call this approach the RBCM with visibility criterion (RBCM-VC).

DOI: 10.1002/nme

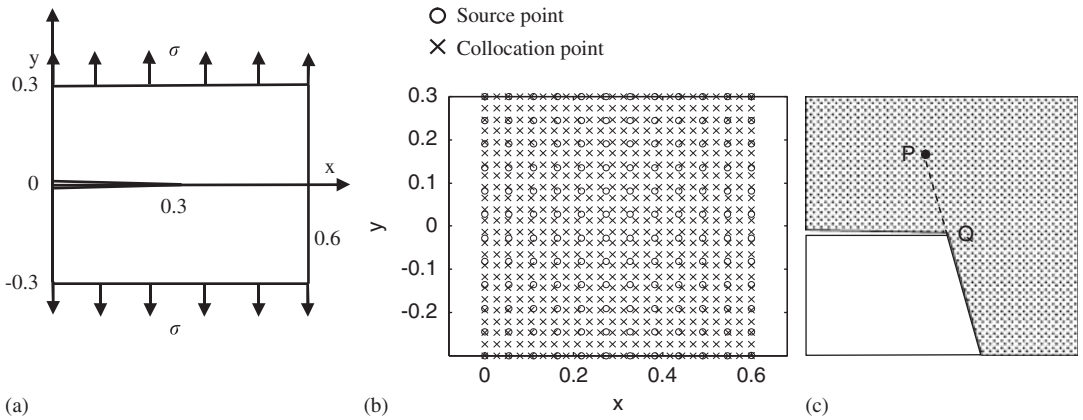

Figure 2. Tensile specimen with edge crack (a) problem statement and (b) RBF discretization, (c) RBF domain of influence (shaded area) of source point P in the cracked domain.

In the numerical test, uniform discretization is employed with different refinements $N_s = 144$, 256, 400. We first use constant shape factors c=0.001 and c=0.4 in RBF. Figure 3(a) and (b) shows the displacement and stress solutions along $y = 0.001$ and indicate that the numerical results converge to a wrong solution. We then use varying shape parameter where smaller c ($c = 0.1r, r$ is the distance from the crack tip) is used near crack tip, and a slight improvement is observed in Figure 3(c). Figure 4 shows the condition numbers of this edge crack problem based on RBCM-VC. The results demonstrate that the condition number of the system increases dramatically for the case with large shape parameter ($c = 0.4$) and the situation can be improved with variable c.

3. SUBDOMAIN RBCM FOR FRACTURE MECHANICS

3.1. Basic equations

We start with the problem statement of a linear elastic fracture mechanics as shown in Figure 5.

$$\nabla \cdot \boldsymbol{\sigma} + \mathbf{b} = 0 \quad \text{in } \Omega \tag{19}$$

$$\mathbf{u} = \bar{\mathbf{u}} \quad \text{on } \partial\Omega_g \tag{20}$$

$$\boldsymbol{\sigma} \cdot \mathbf{n} = \mathbf{t} \quad \text{on } \partial\Omega_t \tag{21}$$

$$\boldsymbol{\sigma} \cdot \mathbf{n} = \mathbf{0} \quad \text{on } \partial\Omega_c \tag{22}$$

where $\partial\Omega_c$ is the crack surface. Equation (19) is the equilibrium equation with $\boldsymbol{\sigma}$ the stress tensor and $\mathbf{b}$ the body force vector. Equations (20)–(22) are boundary conditions with the prescribed displacement $\bar{\mathbf{u}}$, and the surface traction $\mathbf{t}$. The surface traction boundary $\partial\Omega_t$ and the crack surface $\partial\Omega_c$ constitute the Neumann boundary, that is, $\partial\Omega_h = \partial\Omega_t \cup \partial\Omega_c$.

DOI: 10.1002/nme

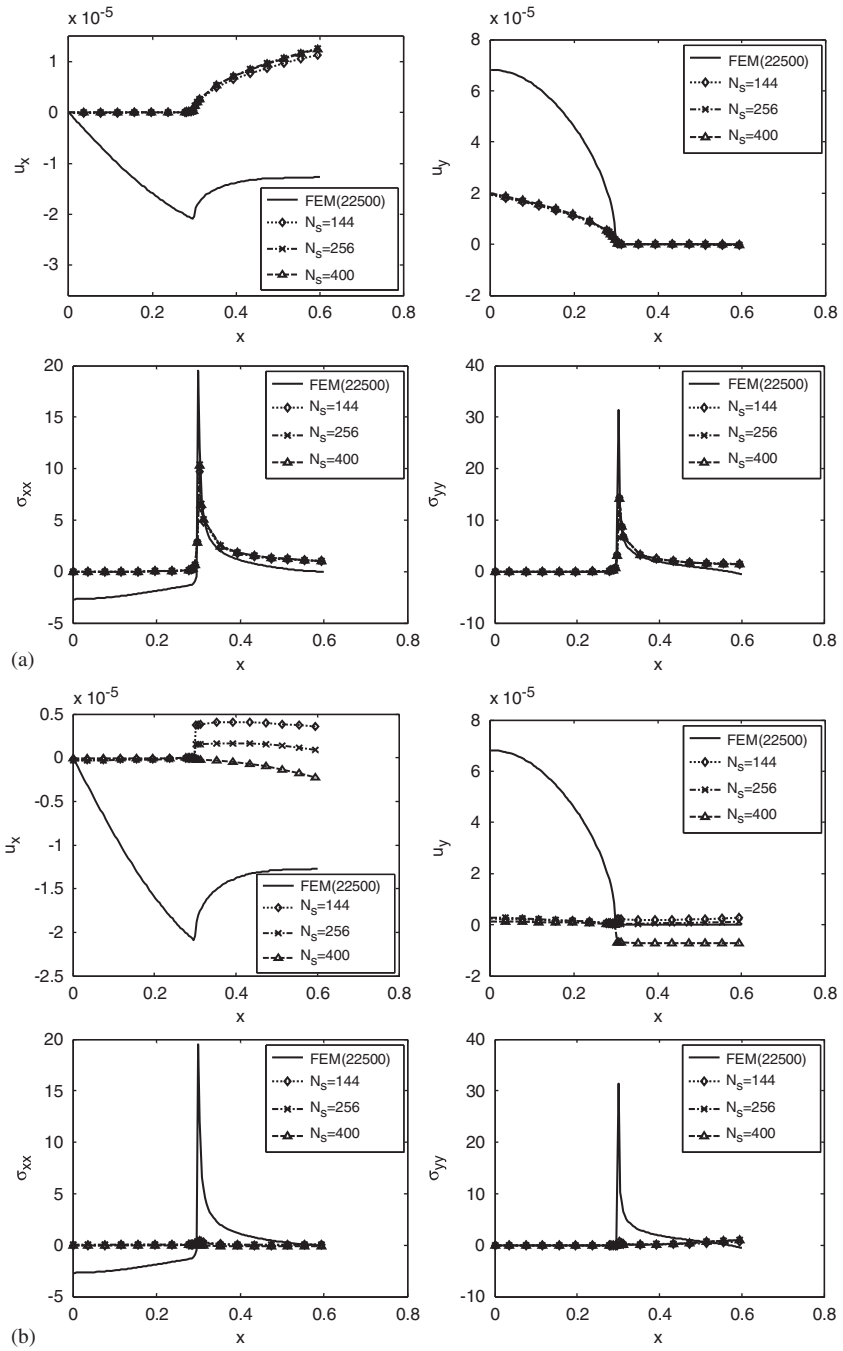

Figure 3. Solution of the edge crack problem along $y=0.001$ obtained from RBCM-VC with: (a) $c=0.001$; (b) $c=0.4$; and (c) varying c.

DOI: 10.1002/nme

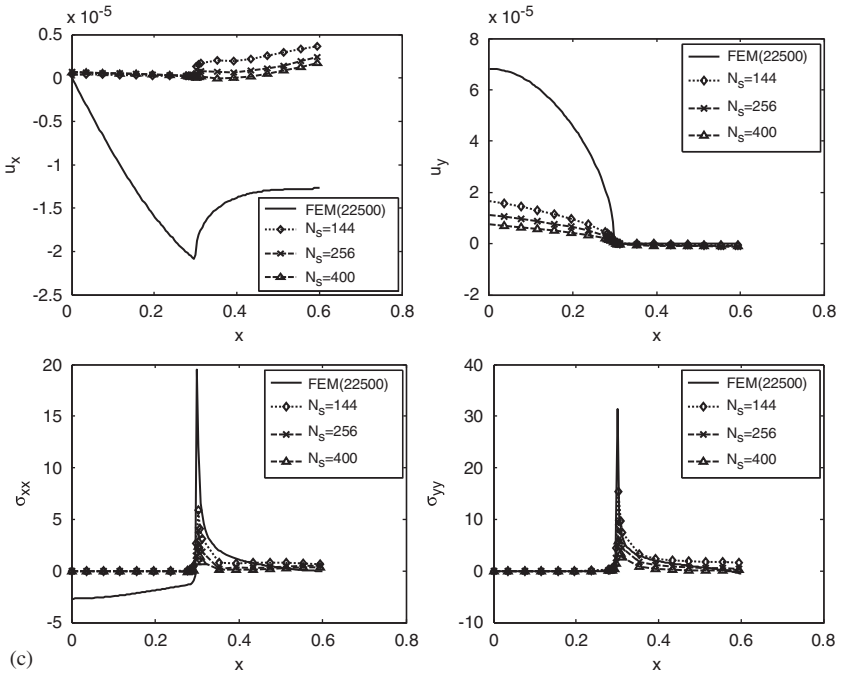

Figure 3. *Continued.*

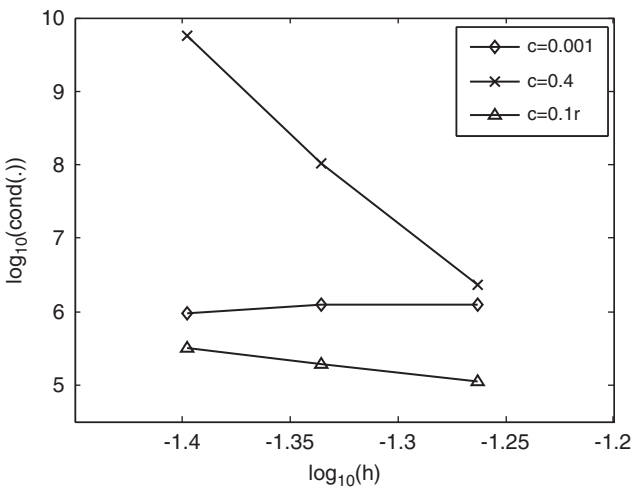

Figure 4. Condition numbers of **A** matrix at different levels of refinement and with different shape parameters.

DOI: 10.1002/nme

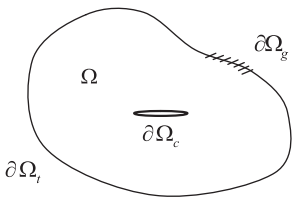

Figure 5. Domain and boundaries of a fracture problem.

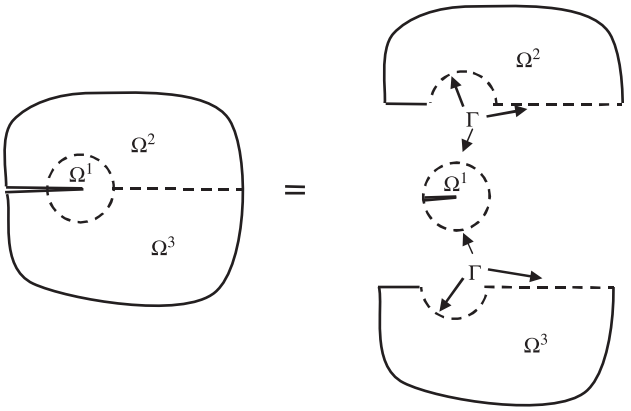

Figure 6. Domain partition in crack problem.

The strong form statement in (19)–(22) can be expressed in the following operator forms:

$$\mathbf{Lu} = \mathbf{f}, \quad \mathbf{f} = \mathbf{b} \quad \text{in } \Omega \tag{23}$$

$$\mathbf{B}_g\mathbf{u} = \mathbf{g}, \quad \mathbf{g} = \bar{\mathbf{u}} \quad \text{on } \partial\Omega_g \tag{24}$$

$$\mathbf{B}_h\mathbf{u} = \mathbf{h}, \quad \mathbf{h} = \begin{cases} \mathbf{t} & \text{on } \partial\Omega_t \\ \mathbf{0} & \text{on } \partial\Omega_c \end{cases} \tag{25}$$

where $\mathbf{L}$ is the differential operator of equilibrium, $\mathbf{B}_g$ and $\mathbf{B}_h$ are the boundary operators associated with prescribed displacement and surface traction boundary conditions, respectively.

3.2. Subdomain collocation

To introduce enrichment functions near crack tip and to represent proper discontinuity across the crack surface in the RBF approximation of the displacement field, we consider a domain partitioning as shown in Figure 6 with separate approximation in each subdomain in conjunction with proper interface conditions on the interface Γ.

DOI: 10.1002/nme

Let $\mathbf{v}^\alpha(\mathbf{x})$ be the approximation of $\mathbf{u}(\mathbf{x})$ for $\mathbf{x}\in\Omega^\alpha$, the subdomain collocation of strong forms is given as

$$\begin{aligned}
\mathbf{L}\mathbf{v}^\alpha(\mathbf{p}_I)&=\mathbf{f}(\mathbf{p}_I),\quad \mathbf{p}_I\in\Omega^\alpha,\quad I=1,\ldots,N_p^\alpha,\quad \alpha=1,2,3\\
\mathbf{B}_g\mathbf{v}^\alpha(\mathbf{q}_I)&=\mathbf{g}(\mathbf{q}_I),\quad \mathbf{q}_I\in\partial\Omega_g\cap\partial\Omega^\alpha,\quad I=1,\ldots,N_q^\alpha,\quad \alpha=1,2,3\\
\mathbf{B}_h\mathbf{v}^\alpha(\mathbf{r}_I)&=\mathbf{h}(\mathbf{r}_I),\quad \mathbf{r}_I\in\partial\Omega_h\cap\partial\Omega^\alpha,\quad I=1,\ldots,N_r^\alpha,\quad \alpha=1,2,3
\end{aligned}\tag{26}$$

with interface conditions

$$\begin{aligned}
\mathbf{v}^+(\mathbf{s}_I)-\mathbf{v}^-(\mathbf{s}_I)&=\mathbf{0}\\
\mathbf{B}_h^+\mathbf{v}^+(\mathbf{s}_I)+\mathbf{B}_h^-\mathbf{v}^-(\mathbf{s}_I)&=\mathbf{0}
\end{aligned},\quad \mathbf{s}_I\in\Gamma,\quad I=1,\ldots,N_\Gamma\tag{27}$$

where $\partial\Omega^\alpha$ is the boundary of subdomain Ω^α, and $\{\mathbf{p}_I\}_{I=1}^{N_p^\alpha}\subseteq\Omega^\alpha$, $\{\mathbf{q}_I\}_{I=1}^{N_q^\alpha}\subseteq\partial\Omega_g\cap\partial\Omega^\alpha$, $\{\mathbf{r}_I\}_{I=1}^{N_r^\alpha}\subseteq\partial\Omega_h\cap\partial\Omega^\alpha$, and $\{\mathbf{s}_I\}_{I=1}^{N_\Gamma}\subseteq\Gamma$ are the collocation points in the subdomain Ω^α, Dirichlet subboundary $\partial\Omega_g\cap\partial\Omega^\alpha$, Neumann subboundary $\partial\Omega_h\cap\partial\Omega^\alpha$, and subdomain interface Γ, respectively. The first interface condition in (27) is the displacement compatibility, where $(\mathbf{v}^+,\mathbf{v}^-)$ denote the approximated displacements of the two subdomains interacting interface Γ, and the second condition in (27) is the operator form of interface traction equilibrium $\sigma_{ij,j}^+n_j^+=\sigma_{ij,j}^-n_j^-$, where σ_{ij}^α and n_j^α are the stress computed by v_i^α in Ω^α and surface normal on $\partial\Omega^\alpha$, respectively.

The RBF approximations of the displacements in each subdomain are constructed as follows:

(i) For the near-tip subdomain ($\alpha=1$):

$$v_i^1(\mathbf{x})=\sum_{I=1}^{N_s^1}\phi_I^1(\mathbf{x})a_{iI}^1+\sum_{I=1}^{4}\hat{\phi}_I(\mathbf{x})\hat{a}_{iI},\quad \mathbf{x}\in\bar{\Omega}^1=\Omega^1\cup\partial\Omega^1\tag{28}$$

(ii) For far-field subdomains ($\alpha=2,3$):

$$v_i^\alpha(\mathbf{x})=\sum_{I=1}^{N_s^\alpha}\phi_I^\alpha(\mathbf{x})a_{iI}^\alpha,\quad \mathbf{x}\in\bar{\Omega}^\alpha=\Omega^\alpha\cup\partial\Omega^\alpha,\quad \alpha=2,3\tag{29}$$

where $N_s^\alpha$is the number of source points in the subdomain $\bar{\Omega}^\alpha=\Omega^\alpha\cup\partial\Omega^\alpha$, $\{\phi_I^\alpha\}_{I=1}^{N_s^\alpha}$ are the set of RBFs with their corresponding source points $\{\mathbf{x}_I^\alpha\}_{I=1}^{N_s^\alpha}$ located in $\bar{\Omega}^\alpha$. As described above, the displacements are approximated by RBFs with enrichment functions $\{\hat{\phi}_I\}_{I=1}^4$ given in (18) in the near-tip subdomain Ω^1, and are approximated by the standard RBFs without enrichment in the far-field subdomains Ω^2 and Ω^3. This subdomain approximation allows enrichment functions be introduced only near the crack tip without affecting far-field solution in finite domain problems. The displacement continuity and traction equilibrium on the subdomain interface $\bar{\Omega}^1\cap(\bar{\Omega}^2\cup\bar{\Omega}^3)$ are enforced by the interface conditions in (27). The subdomain approximation in Ω^2 and Ω^3 with the imposition of interface conditions (27) on $\bar{\Omega}^2\cap\bar{\Omega}^3$ is intended to introduce discontinuity across the crack surface $\partial\Omega_c$.

DOI: 10.1002/nme

3.3. Convergence properties

Let U be finite-dimensional collection of basis functions, $U=\cup_{i=1}^{3} V_i$, where $V_1=\text{span}\{\phi_I, \hat{\phi}_I\}$ and the other subspaces $V_2=V_3=\text{span}\{\phi_I\}$, ϕ_I are RBF defined in Section 2.1, and $\hat{\phi}_I$ are singular functions given in (18). Define a functional

$$
\begin{aligned}
E(\mathbf{v}) = {} & \frac{1}{2}\sum_{\alpha=1}^{3}\int_{\Omega^\alpha}(\mathbf{L}\mathbf{v}^\alpha-\mathbf{f})^2\,\mathrm{d}\Omega+\sum_{\alpha=2}^{3}\frac{w_h^\alpha}{2}\int_{\partial\Omega_h\cap\partial\Omega^\alpha}(\mathbf{B}_h\mathbf{v}^\alpha-\mathbf{h})^2\,\mathrm{d}\Gamma \\
& +\sum_{\alpha=2}^{3}\frac{w_g^\alpha}{2}\int_{\partial\Omega_g\cap\partial\Omega^\alpha}(\mathbf{B}_g\mathbf{v}^\alpha-\mathbf{g})^2\,\mathrm{d}\Gamma+\frac{\bar{w}_g}{2}\sum_{\alpha=2}^{3}\int_{\Gamma}(\mathbf{v}^1-\mathbf{v}^\alpha)^2\mathrm{d}\Gamma \\
& +\frac{\bar{w}_h}{2}\sum_{\alpha=2}^{3}\int_{\Gamma}(\mathbf{B}_h\mathbf{v}^1-\mathbf{B}_h\mathbf{v}^\alpha)^2\,\mathrm{d}\Gamma+\frac{\bar{w}_g}{2}\int_{\Gamma}(\mathbf{v}^2-\mathbf{v}^3)^2\,\mathrm{d}\Gamma+\frac{\bar{w}_h}{2}\int_{\Gamma}(\mathbf{B}_h\mathbf{v}^2-\mathbf{B}_h\mathbf{v}^3)^2\,\mathrm{d}\Gamma \quad (30)
\end{aligned}
$$

The solution for subdomain collocation in (26) can be viewed as minimization of least-squares functional with quadratures: to seek solution $\tilde{\mathbf{u}}_B$ such that

$$
\hat{E}(\tilde{\mathbf{u}}_B)=\min_{\mathbf{v}\in U}\hat{E}(\mathbf{v}) \quad (31)
$$

where $\hat{E}(\mathbf{v})$denotes the discrete functional form of$E(\mathbf{v})$. Consider a norm

$$
\begin{aligned}
\|\mathbf{v}\|_H = {} & \Bigg\{\sum_{\alpha=1}^{3}(\|\mathbf{L}\mathbf{v}^\alpha\|^2_{0,\Omega^\alpha}+w\|\mathbf{v}\|^2_{1,\Omega^\alpha})+\sum_{\alpha=2}^{3}w_h^\alpha\|\mathbf{B}_h\mathbf{v}^\alpha\|^2_{0,\partial\Omega_h\cap\partial\Omega^\alpha}+\sum_{\alpha=2}^{3}w_g^\alpha\|\mathbf{B}_g\mathbf{v}^\alpha\|^2_{0,\partial\Omega_g\cap\partial\Omega^\alpha} \\
& +\bar{w}_g\sum_{\alpha=2}^{3}\|\mathbf{v}^1-\mathbf{v}^\alpha\|^2_{0,\Gamma}+\bar{w}_h\sum_{\alpha=2}^{3}\|\mathbf{B}_h\mathbf{v}^1-\mathbf{B}_h\mathbf{v}^\alpha\|^2_{0,\Gamma}+\bar{w}_g\|\mathbf{v}^2-\mathbf{v}^3\|^2_{0,\Gamma} \\
& +\bar{w}_h\|\mathbf{B}_h\mathbf{v}^2-\mathbf{B}_h\mathbf{v}^3\|^2_{0,\Gamma}\Bigg\}^{1/2} \quad (32)
\end{aligned}
$$

Following the Lax–Milgram lemma [35], we obtain an optimal estimate below

$$
\begin{aligned}
\|\mathbf{u}-\tilde{\mathbf{u}}_B\|_H & \leqslant \inf_{\mathbf{v}\in U}\|\mathbf{u}-\mathbf{v}\|_H \\
& \leqslant \sum_{\alpha=1}^{3}C_1^\alpha\|\mathbf{L}(R_{N_s^\alpha})\|_{0,\Omega^\alpha}+\sum_{\alpha=1}^{3}C_2^\alpha\sqrt{w}\|(R_{N_s^\alpha})\|_{1,\Omega^\alpha}+\sum_{\alpha=2}^{3}C_3^\alpha\sqrt{w_h^\alpha}\|\mathbf{B}_h(R_{N_s^\alpha})\|_{0,\partial\Omega_h\cap\partial\Omega^\alpha} \\
& \quad +\sum_{\alpha=1}^{3}C_4^\alpha\sqrt{w_g^\alpha}\|\mathbf{B}_g(R_{N_s^\alpha})\|_{0,\partial\Omega_g\cap\partial\Omega^\alpha}+\sum_{\alpha=1}^{3}C_5^\alpha\sqrt{\bar{w}_g}\|R_{N_s^\alpha}\|_{0,\Gamma}+\sum_{\alpha=1}^{3}C_6^\alpha\|R_{N_s^\alpha}\|_{1,\Gamma} \quad (33)
\end{aligned}
$$

where $R_{N_s^\alpha}=\mathbf{u}-\mathbf{v}^\alpha$ is the remainder in Ω^α, C_j^α are genetic constants, and triangle inequalities on interior boundary Γ have been used

$$
\sum_{\alpha=2}^{3}\|\mathbf{v}^1-\mathbf{v}^\alpha\|_{0,\Gamma}=\sum_{\alpha=2}^{3}\|\mathbf{v}^1-\mathbf{u}+\mathbf{u}-\mathbf{v}^\alpha\|_{0,\Gamma}\leqslant C\sum_{\alpha=1}^{3}\|\mathbf{u}-\mathbf{v}^\alpha\|_{0,\Gamma} \quad (34)
$$

DOI: 10.1002/nme

Denote $R_{N_s} = \max\{R_{N_s^1}, R_{N_s^2}, R_{N_s^3}\}$. Above error bound can be written as follows:

$$\begin{aligned}\|\mathbf{u}-\tilde{\mathbf{u}}_B\|_H \leqslant\ & C_1\|\mathbf{L}(R_{N_s})\|_{0,\Omega}+C_2\sqrt{w}\|R_{N_s}\|_{1,\Omega}\\ & +C_3\sqrt{w_h}\|\mathbf{B}_h(R_{N_s})\|_{0,\partial\Omega_h\cap\partial\Omega^\alpha}+C_4\sqrt{w_g}\|\mathbf{B}_g(R_{N_s})\|_{0,\partial\Omega_g\cap\partial\Omega^\alpha}\\ & +C_5\|R_{N_s}\|_{1,\Gamma}\end{aligned} \tag{35}$$

Note that both displacement and traction conditions on the interior bounding Γ are needed to get an optimal solution [24].

If there exist exponential convergence rates in each subdomain and on the boundaries, we obtain

$$\|\mathbf{u}-\tilde{\mathbf{u}}_B\|_H \leqslant O(\eta_s^{c/h}) \tag{36}$$

where parameters c and h are addressed in Section 2.1 and $0<\eta_s<1$ is a real number. Accuracy and rate of convergence are determined by the shape parameter c and the number of basis function N_s^α in each subdomain Ω^α. If the particular solutions are used as the admissible functions, this leads to the collocation Trefftz method [31, 33], and there exist exponential convergence rates as well.

3.4. Coupling strategy from convergence consideration

Consider a second-order operator $\mathbf{L}=\boldsymbol{\Delta}$, the tracing inequalities are

$$\|\mathbf{v}\|_{1,\Gamma} \leqslant C_0\|\mathbf{v}\|_{2,\Omega}, \tag{37}$$

$$\|\mathbf{v}\|_{0,\Gamma} \leqslant \tilde{C}_0\|\mathbf{v}\|_{1,\Omega}, \tag{38}$$

The error bound in (35) can then be written as follows:

$$\begin{aligned}\|\mathbf{u}-\tilde{\mathbf{u}}_B\|_H &\leqslant C_1\|R_{N_s^1}\|_{2,\Omega^1}+C_2\|R_{N_s^2}\|_{2,\Omega^2}+C_3\|R_{N_s^3}\|_{2,\Omega^3}\\ &\leqslant C_1\eta_1^{c/h_1}\|u\|_t+C_2\eta_2^{c/h_2}\|u\|_t+C_3\eta_3^{c/h_3}\|u\|_t\end{aligned} \tag{39}$$

where $R_{N_s^\alpha}$ is the remainder in Ω^α, $0<\eta_\alpha<1$, $\alpha=1,2,3$ and $\|\cdot\|_t$ is induced form defined in [11]. We define the nodal distances h_α in each subdomain Ω^α as

$$h_\alpha=\left(\frac{\text{Area}(\Omega^\alpha)}{N_s^\alpha}\right)^{1/n} \quad \text{in } n\text{-dimension} \tag{40}$$

According to Equation (39), for balance of errors among the three subdomains, we consider

$$\eta_1^{c/h_1}\approx\eta_\alpha^{c/h_\alpha} \quad \text{where } \alpha=2,3 \tag{41}$$

Taking nature log of each side, we obtain the relationship

$$(c/h_1)\log\eta_1\approx(c/h_\alpha)\log\eta_\alpha \quad \text{where } \alpha=2,3 \tag{42}$$

Substituting (40) into (42), we obtain

$$\frac{N_s^1}{\text{Area}(\Omega^1)}=\left(\frac{\log\eta_\alpha}{\log\eta_1}\right)^n\frac{N_s^\alpha}{\text{Area}(\Omega^\alpha)} \tag{43}$$

DOI: 10.1002/nme

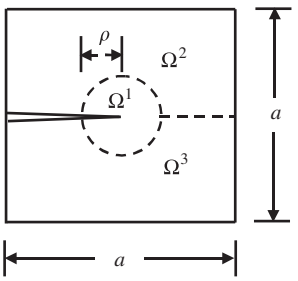

Figure 7. Domain partition for concave domain.

or

$$N_s^\alpha = \left(\frac{\log \eta_1}{\log \eta_\alpha}\right)^n \frac{\text{Area}(\Omega^\alpha)}{\text{Area}(\Omega^1)} N_s^1 \tag{44}$$

Based on the number of basis functions used in each subdomain, the optimal dimension of the near-tip subdomain Ω^1 can be estimated. As shown in Figure 7, if the number of basis functions is proportional to the area of subdomains, we have

$$\frac{\pi\rho^2}{(a^2-\pi\rho^2)/2} = \frac{N_s^1}{\bar{N}_s}, \quad \bar{N}_s = \min(N_s^2, N_s^3) \tag{45}$$

where ρ denotes the radius of subdomain Ω^1, and a is the dimension of the plate patch. Thus, we obtain the relationship for selection of the radius of subdomain Ω^1:

$$\rho = \sqrt{\frac{\beta a^2}{(2+\beta)\pi}} \quad \text{where } \beta = \frac{N_s^1}{\bar{N}_s} \tag{46}$$

4. NUMERICAL EXAMPLES

In the following numerical examples, the collocation method applied to the strong forms of each subdomain augmented with interface conditions as given in Equations (26)–(27) is introduced. The approximation of solution in each subdomain by RBFs and with enrichment functions introduced in the near-tip subdomain as described in Equations (28)–(29) is employed. We call this proposed method as the SD-RBCM. MQ RBFs are used for all the numerical examples. To achieve optimal solution accuracy, weighted collocation method [10] is introduced to balance the errors in the domain and on the boundaries. The collocation equations for the boundary and interface are weighted as follows:

Subdomain strong forms:

$$\begin{aligned}
&\mathbf{L}\mathbf{v}^\alpha(\mathbf{p}_I) = \mathbf{f}(\mathbf{p}_I), \quad \mathbf{p}_I \in \Omega^\alpha, \quad I = 1, \ldots, N_p^\alpha, \quad \alpha = 1, 2, 3 \\
&\sqrt{w_g^\alpha}\mathbf{B}_g\mathbf{v}^\alpha(\mathbf{q}_I) = \sqrt{w_g^\alpha}\mathbf{g}(\mathbf{q}_I), \quad \mathbf{q}_I \in \partial\Omega_g \cap \partial\Omega^\alpha, \quad I = 1, \ldots, N_q^\alpha, \quad \alpha = 1, 2, 3 \\
&\sqrt{w_h^\alpha}\mathbf{B}_h\mathbf{v}^\alpha(\mathbf{r}_I) = \sqrt{w_h^\alpha}\mathbf{h}(\mathbf{r}_I), \quad \mathbf{r}_I \in \partial\Omega_h \cap \partial\Omega^\alpha, \quad I = 1, \ldots, N_r^\alpha, \quad \alpha = 1, 2, 3
\end{aligned} \tag{47}$$

DOI: 10.1002/nme

Interface conditions:

$$\begin{aligned} \sqrt{\bar{w}_g}(\mathbf{v}^+(\mathbf{s}_I)-\mathbf{v}^-(\mathbf{s}_I))&=\mathbf{0} \\ \sqrt{\bar{w}_h}(\mathbf{B}_h^+\mathbf{v}^+(\mathbf{s}_I)+\mathbf{B}_h^-\mathbf{v}^-(\mathbf{s}_I))&=\mathbf{0}, \quad \mathbf{s}_I\in\Gamma, \quad I=1,\ldots,N_\Gamma \end{aligned} \tag{48}$$

The weights suggested by Chen *et al*. [24] are:

$$\sqrt{w_g^\alpha}=\sqrt{\bar{w}_g}=O(\bar{k}\cdot\bar{N}_s), \quad \sqrt{w_h^\alpha}=O(s^\alpha), \quad \sqrt{\bar{w}_h}=O(1) \tag{49}$$

where $\bar{k}=\max\{k^\alpha\}$, $k^\alpha=\max\{\lambda^\alpha,\mu^\alpha\}$, $\bar{N}_s=\max\{N_s^\alpha\}$, $s^\alpha=\bar{k}/k^\alpha$, λ^α and μ^α are Lame's constants in $\bar{\Omega}^\alpha$ and N_s^α is the number of source points in $\bar{\Omega}^\alpha$.

4.1. The variant Motz's problem

A two dimensional variant Motz's problem is given as

$$\Delta u=\frac{\partial^2 u}{\partial x^2}+\frac{\partial^2 u}{\partial y^2}=0 \quad \text{in } \Omega \tag{50}$$

where $\Omega=\{(x,y)|-1/2\leqslant x\leqslant 1/2, 0\leqslant y\leqslant 1/2\}$ as shown in Figure 8, and the following mixed Dirichlet-Neumann boundary conditions are introduced

$$\begin{aligned} \frac{\partial u}{\partial x}&=0 \quad \text{on } x=-\frac{1}{2}\cap 0\leqslant y\leqslant\frac{1}{2}, \\ u&=0.125 \quad \text{on } y=\frac{1}{2}\cap -\frac{1}{2}\leqslant x\leqslant\frac{1}{2}, \\ \frac{\partial u}{\partial x}&=0 \quad \text{on } x=\frac{1}{2}\cap 0\leqslant y\leqslant\frac{1}{2}, \\ \frac{\partial u}{\partial y}&=0 \quad \text{on } y=0\cap 0<x\leqslant\frac{1}{2}, \\ u&=0 \quad \text{on } y=0\cap\frac{1}{2}\leqslant x<0. \end{aligned} \tag{51}$$

The discontinuity of boundary conditions at $(0,0)$ yields a singularity $u=O(\sqrt{r})$ as $r\to 0$. A series solution has been proposed [31]:

$$u(r,\theta)=\sum_{i=0}^{\infty} d_i r^{i+1/2}\cos\left(i+\frac{1}{2}\right)\theta \tag{52}$$

The domain partitioning of this problem is shown in Figure 9, where Ω^1 with radius $\rho=0.1$ is used. In this problem, only the first term in the series solution, $\sqrt{r}\cos(\theta/2)$, is used as the enrichment function in the near-tip subdomain Ω^1 together with RBF bases, and only RBFs are used as the

DOI: 10.1002/nme

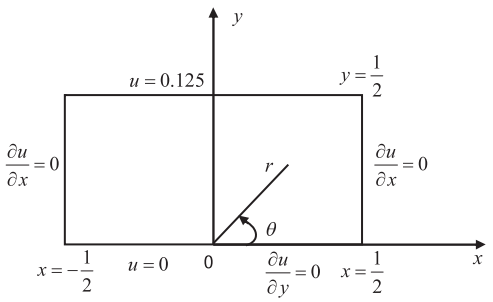

Figure 8. The variant Motz's problem definition.

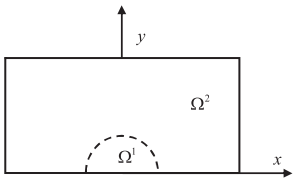

Figure 9. Domain partitioning of the variant Motz's problem.

bases in the far-field subdomain Ω^2, that is,

$$v^1(\mathbf{x}) = \sum_{I=1}^{N_s^1} \phi_I^1(\mathbf{x}) a_I^1 + \sqrt{r}\cos(\theta/2)\hat{a}, \quad \mathbf{x} \in \bar{\Omega}^1 = \Omega^1 \cup \partial\Omega^1 \tag{53}$$

$$v^2(\mathbf{x}) = \sum_{I=1}^{N_s^2} \phi_I^2(\mathbf{x}) a_I^2, \quad \mathbf{x} \in \bar{\Omega}^2 = \Omega^2 \cup \partial\Omega^2 \tag{54}$$

A total of 18 source points are used in $\bar{\Omega}^1$, and 240 source points are used in $\bar{\Omega}^2$. Consequently, 4×18 and 4×240 collocation points are used in $\bar{\Omega}^1$ and $\bar{\Omega}^2$, respectively. The weights for the boundary collocation equations are introduced based on (49) with $\bar{k} = 1$.

Figure 10 shows that the best accuracy in the solution and its derivatives along $y = 0.001$ can be obtained by SD-RBCM with radius $\rho = 0.1$ for $\bar{\Omega}^1$. According to (46), the prediction of the optimal dimension of near-tip subdomain is $\rho = 0.105$, and the numerical results in Figure 10 are consistent with this prediction. Further, with the same discretization, the condition number of the matrix in the discrete equation is reduced from 10^{17} for the case without domain partitioning to 10^{12} for the SD-RBCM with subdomain approximation.

4.2. Edge crack in a square plate subjected to tension

We revisit the crack problem discussed in Section 3 and compare the results of RBCM and RBCM-VC with the proposed SD-RBCM approach. The domain partitioning of this problem is described in Figure 11 with the radius for the near-tip subdomain being $\rho = 0.1$. In the SD-RBCM approach, MQ RBFs and enrichment functions are used to approximate displacements in subdomain $\bar{\Omega}^1$,

DOI: 10.1002/nme

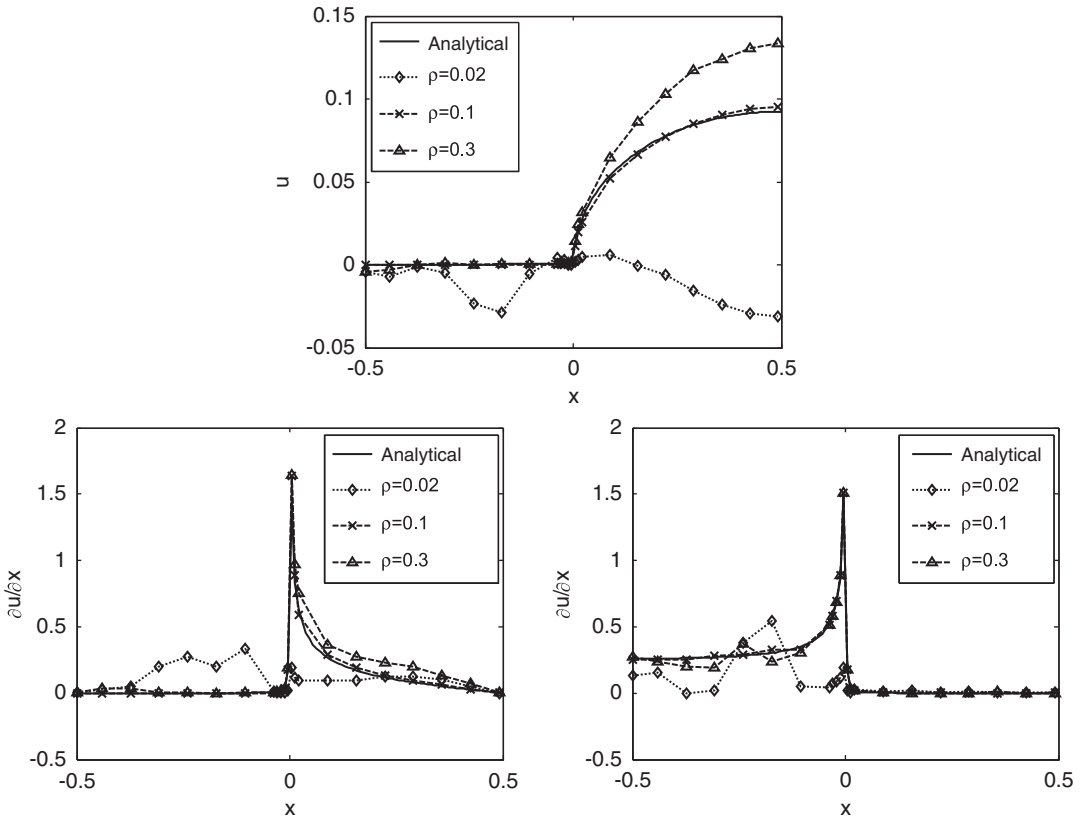

Figure 10. Solution of the variant Motz's problem at $y=0.001$.

whereas only MQ RBFs are used in subdomains $\bar{\Omega}^2$ and $\bar{\Omega}^3$. The number of source points and collocation points used in each subdomain are $N_s^1=26$, $N_s^2=N_s^3=150$, and $N_c^\alpha=4N_s^\alpha$, $\alpha=1,2,3$, respectively as shown in Figure 17.

Solution obtained by finite element method with 22 500 elements is used as the reference solution of this problem. The comparison of displacement and stress solutions in Figure 12 demonstrates the significant accuracy improvement in SD-RBCM compared with the solution of RBCM with or without visibility criterion. The condition numbers of the discrete equation associated with different methods are compared in Figure 13. The results show that SD-RBCM discrete systems are much well-conditioned compared with those of RBCM-based approaches without subdomain approximation.

The convergence of the solution in L_2 and H^1 norms shown in Figure 14 also exhibits a much higher convergence rates in SD-RBCM compared with the RBCM-based approaches. The effect of near-tip subdomain dimension on the solution accuracy is shown in Figure 15. The results suggest that an optimal dimension of near-tip subdomain exists in this finite domain problem. The numerical tests validate the result obtained from (46), which gives the optimal radius of near-tip subdomain to be $\rho=0.096$.

DOI: 10.1002/nme

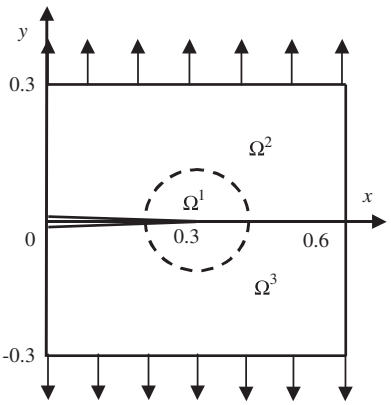

Figure 11. Domain partition in SD-RBCM.

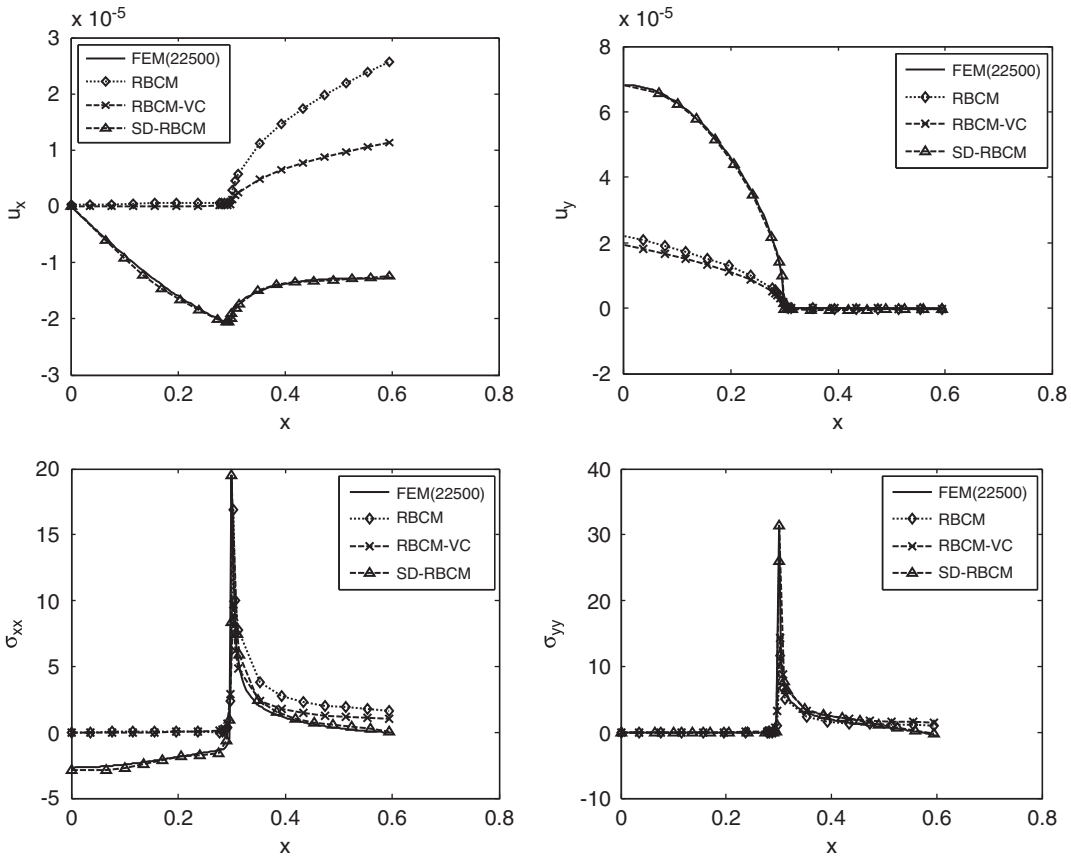

Figure 12. Comparison of solution at $y=0.001$ of the edge crack plate subjected to tension.

DOI: 10.1002/nme

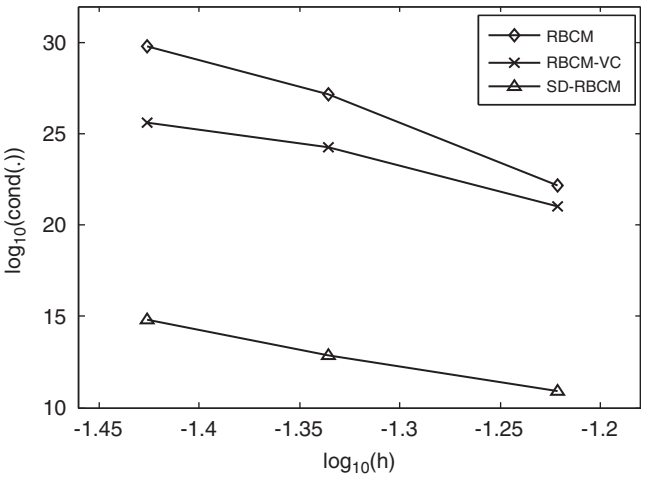

Figure 13. Condition number of the **A** matrix in the edge crack plate subjected to tension using RBCM, RBCM-VC, and SD-RBCM.

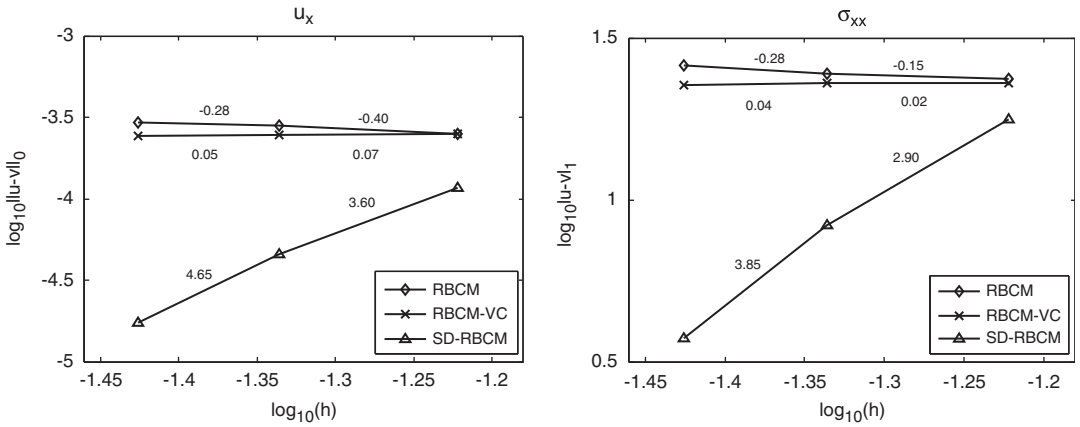

Figure 14. Convergence of L_2 and H_1 error norms of the edge crack plate subjected to tension.

We assume that the error exhibits an exponential convergence behavior as

$$\varepsilon = C\eta^{cN}, \quad 0<\eta<1 \tag{55}$$

where N denotes the number of source points in one direction and c is the RBF shape parameter. Express errors in two levels of discretization as:

$$\varepsilon_1 = C\eta^{c_1 N_1}, \quad \varepsilon_2 = C\eta^{c_2 N_2}. \tag{56}$$

It follows that

$$\eta = \mathrm{e}^{(\log\varepsilon_1 - \log\varepsilon_2)/(c_1 N_1 - c_1 N_2)} \tag{57}$$

DOI: 10.1002/nme

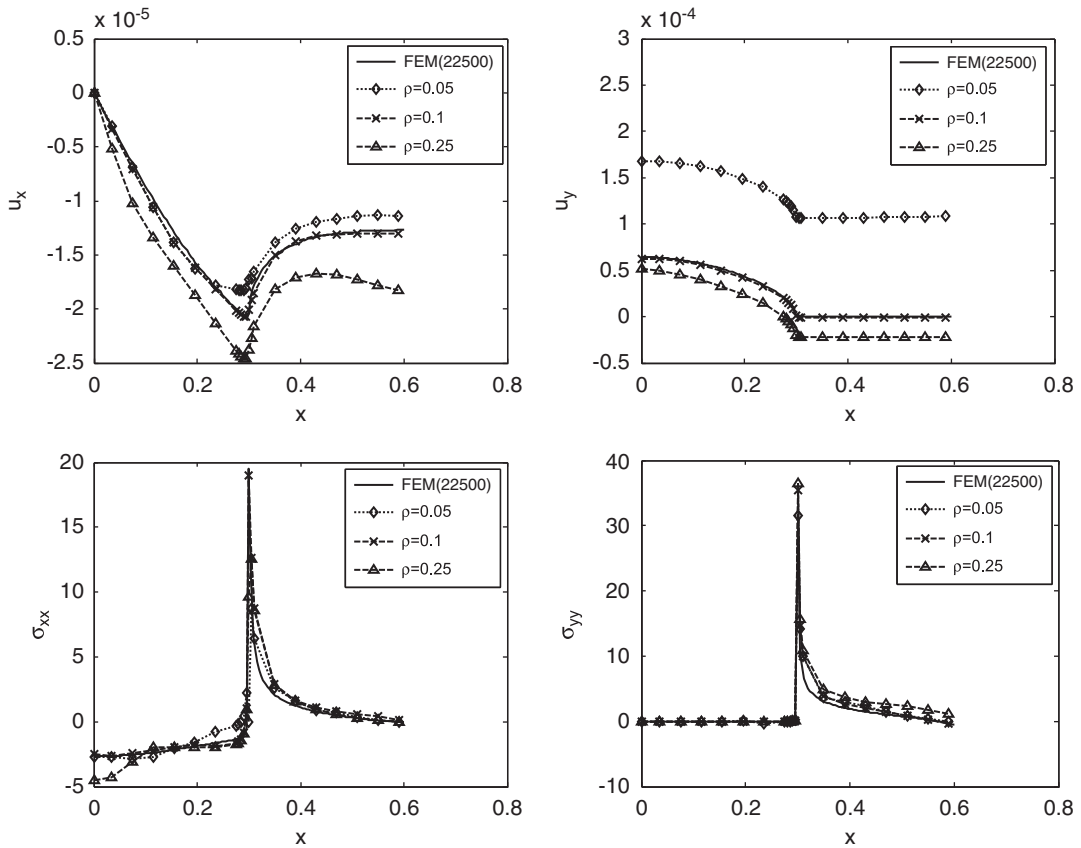

Figure 15. Solution at $y=0.001$ of the edge crack plate subjected to tension using different near-tip subdomain radii.

We use this formula to calculate the asymptotic error behavior as follows:

(1) For RBCM:

$$\|u-v\|_{0,\Omega}\approx O((1.14)^{cN}),\quad \|u-v\|_{1,\Omega}\approx O((1.09)^{cN}) \tag{58}$$

(2) For RBCM-VC:

$$\|u-v\|_{0,\Omega}\approx O((0.98)^{cN}),\quad \|u-v\|_{1,\Omega}\approx O((0.99)^{cN}) \tag{59}$$

(3) For SD-RBCM:

$$\|u-v\|_{0,\Omega}\approx O((0.20)^{cN}),\quad \|u-v\|_{1,\Omega}\approx O((0.27)^{cN}) \tag{60}$$

Equations (58)–(60) indicate that RBCM does not converge, RBCM-VC has very slow convergence, and SD-RBCM has the exponential convergence.

DOI: 10.1002/nme

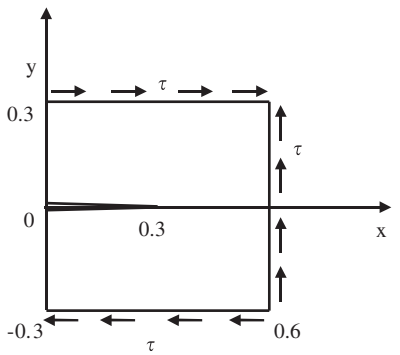

Figure 16. Edge crack in a finite plate under shear.

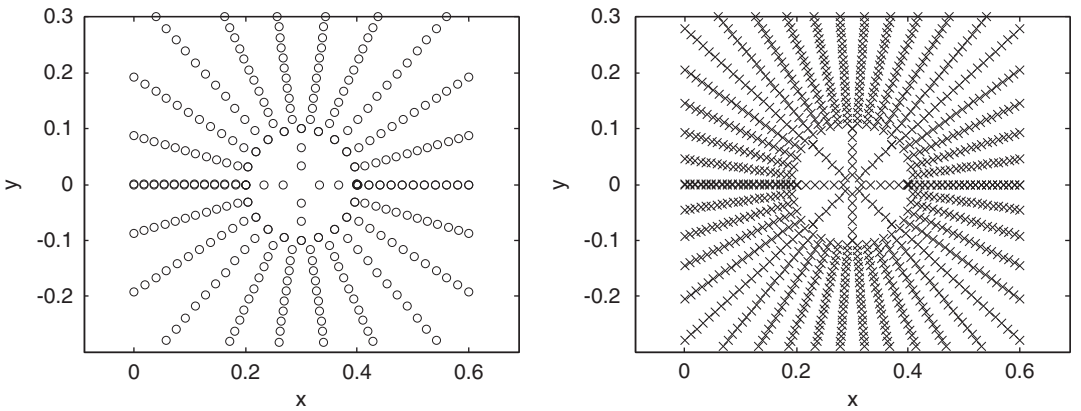

Figure 17. Source points and collocation points used in the discretization.

4.3. Edge crack in a finite plate subjected to shear load

Consider a crack subjected to shear load in a finite domain as displayed in Figure 16. The dimension of the patch is 0.6×0.6, and the crack length is 0.3. The material properties of the plate are Young's modulus $E=3\times10^4$ and the Poisson ratio $\nu=0.3$. The applied shear load is $\tau=1.0$. The domain partitioning of this problem is similar to that in Figure 11 with the radius for the near-tip subdomain being $\rho=0.1$ and similar discretization as described in Figure 17 is employed.

Solution based on finite element method with 23 280 elements is used as the reference solution for this problem. Once again, the numerical results in Figure 18 show a good accuracy obtained from SD-RBCM compared with the solutions of RBCM and RBCM-VC. Owing to the use of same discretization as that of Example 4.2, same condition numbers as shown in Figure 13 are expected for this problem.

The errors of the solution in L_2 and H^1 error norms in Figure 19 show an exponential convergence in SD-RBCM, very slow convergence rate for RBCM-VC and no convergence in RBCM. The effect of near-tip subdomain dimension on the solution accuracy is compared in Figure 20,

DOI: 10.1002/nme

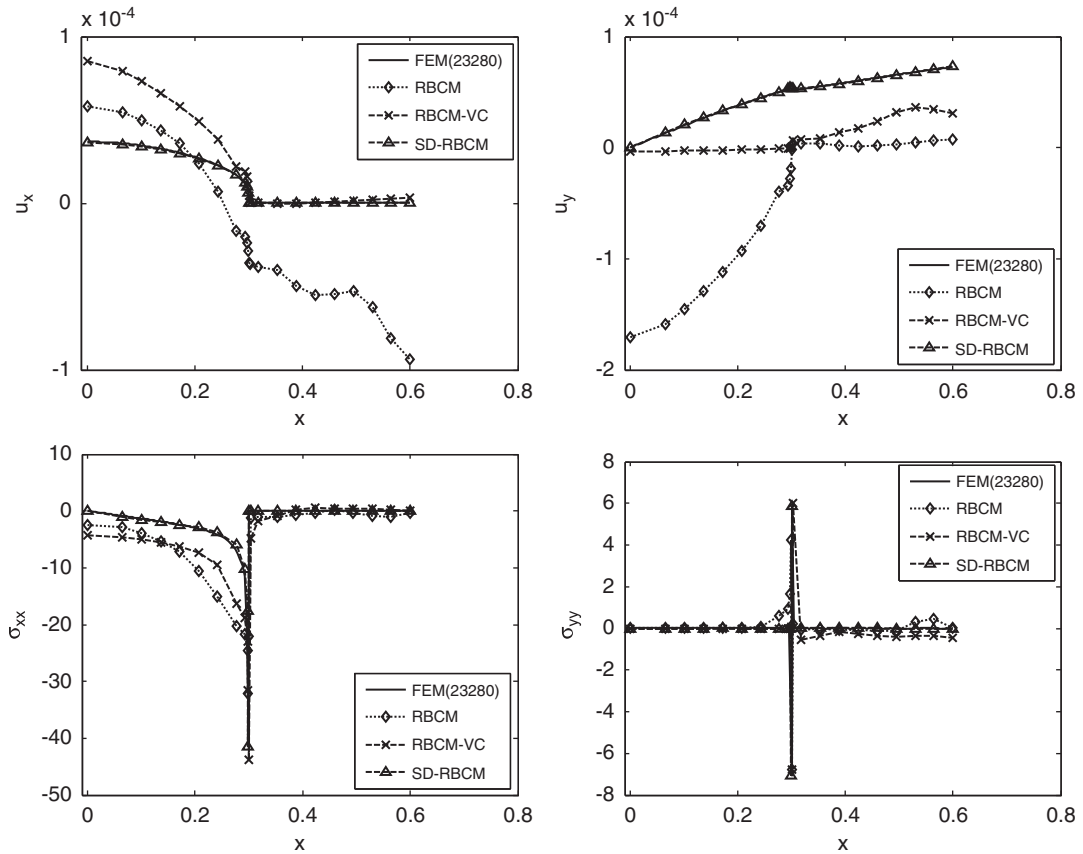

Figure 18. Comparison of solution at $y=0.001$ of the edge crack plate under shear.

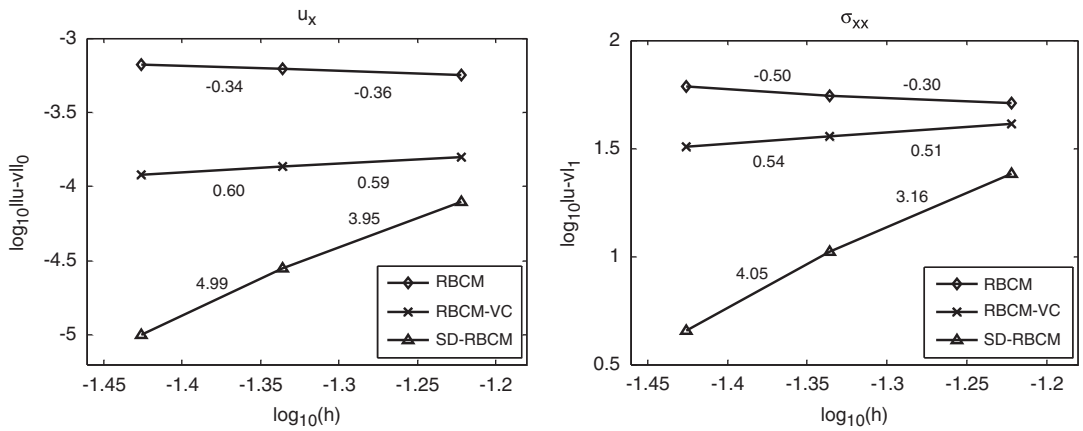

Figure 19. Convergence of L_2 and H_1 error norms of the edge crack plate under shear.

DOI: 10.1002/nme

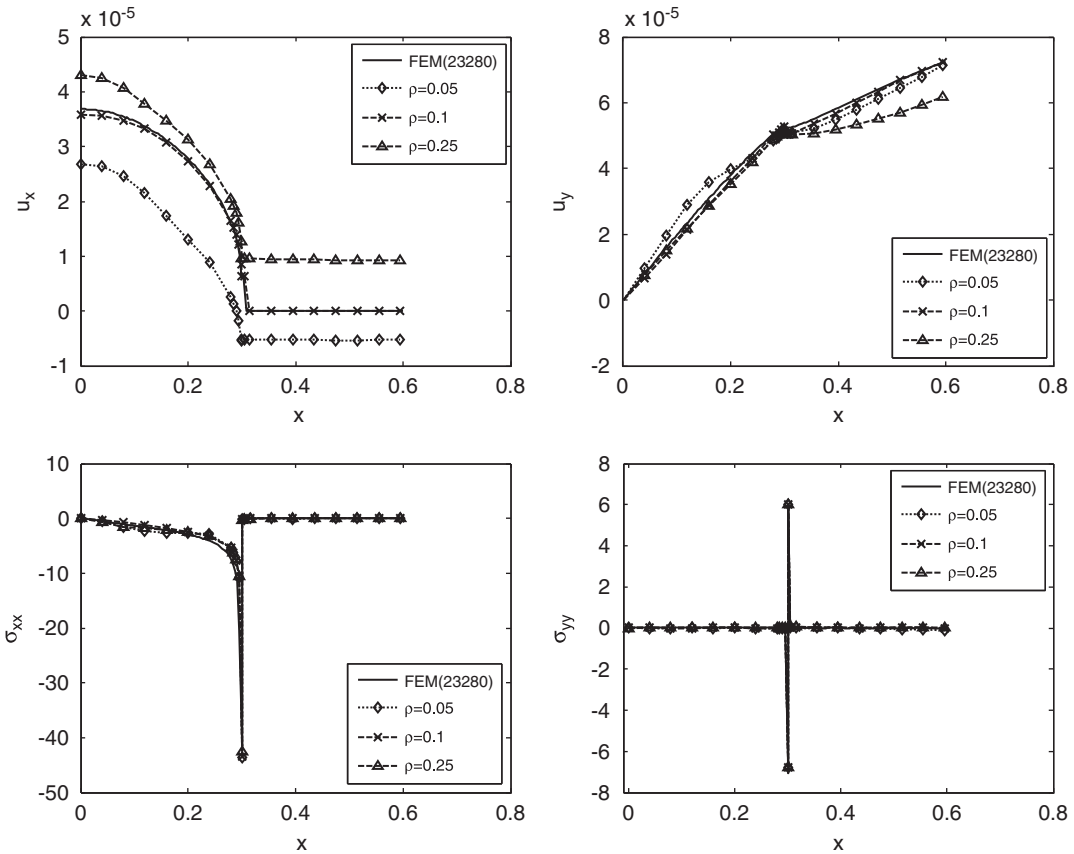

Figure 20. Solution at $y = 0.001$ of the edge crack plate under shear using different near-tip subdomain radii.

which again suggests that a dimension for the near-tip subdomain based on (46) yields the best solution.

5. CONCLUSIONS

Radial basis collocation method (RBCM) for solving PDEs has been an active subject in the past decade. The simplicity of the direct collocation on strong forms and the exponential convergence in the radial basis approximation makes RBCM an attractive computational method. Nevertheless, the nonlocality and the smooth nature of RBFs present intrinsic difficulties in dealing with problems with non-convex geometry and local features, where fracture mechanics is one such example.

The objective of this paper is to introduce an enhanced RBCM to circumvent the above-mentioned difficulties. Since RBFs are typically with high-order smoothness, the crack-tip singularity in stress field and the discontinuity across the crack surface cannot be properly approximated by RBFs. Enrichment functions representing near-tip characteristics commonly used

DOI: 10.1002/nme

in the Galerkin-based method also cannot be easily introduced in the nonlocal RBF approximation. Further, methods such as visibility criterion and other related methods commonly used in meshfree methods with compact supports for crack problems are not applicable due to the nonlocality of RBFs.

In this work we introduced an SD-RBCM originally introduced for heterogeneous materials [24] as an improvement of RBCM for crack problems. By a proper partitioning of the problem domain into subdomains and by introducing separate approximation in each subdomain, the near-tip stress singularity and crack surface displacement discontinuity can be accurately approximated. An important step in this approach is the imposition of displacement continuity and traction equilibrium along the interfaces between adjacent subdomains. We show that with the proper imposition of interface conditions and with suitable weights applied to the boundary and interface collocation equations, an exponential convergence can be obtained. We also show that an optimal dimension of the near-tip subdomain exists in the finite domain crack problems, and this dimension has been analytically derived and numerically validated.

APPENDIX A

Matrices and vectors of strong form collocation in Equation (11):

$$\mathbf{A}_L = \begin{bmatrix} \mathbf{L}\boldsymbol{\Phi}^{\mathrm{T}}(\mathbf{p}_1) \\ \vdots \\ \mathbf{L}\boldsymbol{\Phi}^{\mathrm{T}}(\mathbf{p}_{N_p}) \end{bmatrix}, \quad \mathbf{A}_g = \begin{bmatrix} \mathbf{B}_g\boldsymbol{\Phi}^{\mathrm{T}}(\mathbf{q}_1) \\ \vdots \\ \mathbf{B}_g\boldsymbol{\Phi}^{\mathrm{T}}(\mathbf{q}_{N_q}) \end{bmatrix}, \quad \mathbf{A}_h = \begin{bmatrix} \mathbf{B}_h\boldsymbol{\Phi}^{\mathrm{T}}(\mathbf{r}_1) \\ \vdots \\ \mathbf{B}_h\boldsymbol{\Phi}^{\mathrm{T}}(\mathbf{r}_{N_r}) \end{bmatrix} \tag{A1}$$

$$\mathbf{b}_L = \begin{bmatrix} \mathbf{f}(\mathbf{p}_1) \\ \vdots \\ \mathbf{f}(\mathbf{p}_{N_p}) \end{bmatrix}, \quad \mathbf{b}_g = \begin{bmatrix} \mathbf{g}(\mathbf{q}_1) \\ \vdots \\ \mathbf{g}(\mathbf{q}_{N_q}) \end{bmatrix}, \quad \mathbf{b}_h = \begin{bmatrix} \mathbf{h}(\mathbf{r}_1) \\ \vdots \\ \mathbf{h}(\mathbf{r}_{N_r}) \end{bmatrix} \tag{A2}$$

ACKNOWLEDGEMENTS

The support of this work by National Natural Science Foundation of China (NSFC) under Project No. 10572104 to the first author, the support by US Army ERDC under contract W912HZ-07-C-0019 to the second author, and the support by National Science Council of Taiwan, R. O. C., under project number NSC 96-2115-M-029-002-MY2 to the third author are greatly acknowledged.

REFERENCES

1. Hardy RL. Multiquadric equations of topography and other irregular surfaces. *Journal of Geophysics Research* 1971; **176**:1905–1915.
2. Carlson RE, Foley TA. Interpolation of track data with radial basis methods. *Computers and Mathematics with Application* 1992; **24**:27–34.
3. Wu ZM, Schaback R. Local error estimates for radial basis function interpolation of scattered data. *IMA Journal of Numerical Analysis* 1993; **13**:13–27.

DOI: 10.1002/nme

4. Franke R. Scattered data interpolation: tests of some methods. *Mathematics of Computation* 1982; **98**:181–200.
5. Kansa EJ. Multiqudrics—a scattered data approximation scheme with applications to computational fluid-dynamics—I. Surface approximations and partial derivatives. *Computers and Mathematics with Application* 1990; **19**:127–145.
6. Kansa EJ. Multiqudrics—a scattered data approximation scheme with applications to computational fluid-dynamics—II. Solutions to parabolic, hyperbolic and elliptic partial differential equations. *Computers and Mathematics with Application* 1990; **19**:147–161.
7. Hon YC, Schaback R. On unsymmetric collocation by radial basis functions. *Applied Mathematics and Computation* 2001; **119**:177–186.
8. Fasshauer GE. Solving differential equations with radial basis functions: multilevel methods and smoothing. *Advances in Computational Mathematics* 1999; **11**:139–159.
9. Hu HY, Li ZC, Cheng AHD. Radial basis collocation method for elliptic equations. *Computers and Mathematics with Application* 2005; **50**:289–320.
10. Hu HY, Chen JS, Hu W. Weighted radial basis collocation method for boundary value problems. *International Journal for Numerical Methods in Engineering* 2007; **69**:2736–2757.
11. Madych WR, Nelson SA. Bounds on multivariate polynomials and exponential error estimates for multiquadric interpolation. *Journal of Approximation Theory* 1992; **70**:94–114.
12. Hardy RL. Theory and applications of the multiquadric-biharmonic method: 20 years of discovery. *Computers and Mathematics with Application* 1990; **19**(8/9):163–208.
13. Franke R, Schaback R. Solving partial differential equations by collocation using radial functions. *Applied Mathematics and Computation* 1998; **93**:73–82.
14. Madych WR. Miscellaneous error bounds for multiquadric and related interpolatory. *Computers and Mathematics with Application* 1992; **24**(12):121–138.
15. Wendland H. Meshless Galerkin methods using radial basis functions. *Mathematics of Computation* 1999; **68**(228):1521–1531.
16. Wendland H. Piecewise polynomial, positive definite and compactly supported radial functions of minimal degree. *Advances in Computational Mathematics* 1995; **4**:389–396.
17. Schaback R, Wendland H. Using compactly supported radial basis functions to solve partial differential equations. *Boundary Element Technology XIII*. WIT Press: Southampton, Boston, 1999; 311–324.
18. Xiao JR, McCarthy MA. A local heaviside weighted meshless method for two-dimensional solids using radial basis function. *Computational Mechanics* 2003; **31**:301–315.
19. Liu GR, Gu YT. A local radial point interpolation method (LRPIM) for free vibration analyses of 2-D solids. *Journal of Sound and Vibration* 2001; **246**:29–46.
20. Shu C, Ding H, Yeo KS. Local radial basis function-based differential quadrature method and its application to solve two-dimensional incompressible Navier–Stokes equations. *Computer Methods in Applied Mechanics and Engineering* 2003; **192**:941–954.
21. Chen JS, Hu W, Hu HY. Reproducing kernel enhanced local radial basis collocation method. *International Journal for Numerical Methods in Engineering* 2008; **75**:600–627.
22. Cordes LW, Moran B. Treatment of material discontinuity in the element-free Galerkin method. *Computer Methods in Applied Mechanics and Engineering* 1996; **139**:75–89.
23. Wang D, Chen JS, Sun L. Homogenization of magnetostrictive particle-filled elastomers using an interface-enriched reproducing kernel particle method. *Journal of Finite Element Analysis and Design* 2003; **39**:765–782.
24. Chen JS, Wang L, Hu HY, Chi SW. Subdomain radial basis collocation method for heterogeneous media. *International Journal for Numerical Methods in Engineering* 2009; DOI: 10.1002/nme.2624.
25. Krysl P, Belytschko T. Element-free Galerkin: convergence of the continuous and discontinuous shape functions. *Computer Methods in Applied Mechanics and Engineering* 1997; **148**:257–277.
26. Organ DJ, Fleming M, Terry T, Belytschko T. Continuous meshless approximations for nonconvex bodies by diffraction and transparency. *Computational Mechanics* 1996; **18**:225–235.
27. Fleming M, Chu YA, Moran B, Belytschko T. Enriched element-free Galerkin methods for crack tip fields. *International Journal for Numerical Methods in Engineering* 1997; **40**:1483–1504.
28. Belytschko T, Lu YY, Gu L. Element-free Galerkin methods. *International Journal for Numerical Methods in Engineering* 1994; **37**:229–256.
29. Moes N, Dolbow J, Belytschko T. A finite element method for crack growth without remeshing. *International Journal for Numerical Methods in Engineering* 1999; **46**:131–150.

30. Dolbow J. An extended finite element method with discontinuous enrichment for applied mechanics. *Ph.D. Thesis*, Theoretical and Applied Mechanics, Northwestern University, Evanston, IL, 1999.
31. Lu TT, Hu HY, Li ZC. Highly accurate solutions of Motz's and the cracked beam problems. *Engineering Analysis with Boundary Elements* 2004; **28**:1387–1403.
32. Lee SH, Yoon YC. Meshfree point collocation method for elasticity and crack problems. *International Journal for Numerical Methods in Engineering* 2004; **61**:22–48.
33. Li ZC, Lu TT, Hu HY, Cheng AHD. *Tretftz and Collocation Methods*. WIT Press: Southampton, Boston, 2008.
34. Girosi F. On some extensions of radial basis functions and their applications in artificial intelligence. *Computers and Mathematics with Applications* 1992; **24**:61–80.
35. Ciarlet PG. *The Finite Element Method for Elliptic Problem*. North-Holland Inc.: New York, 1978.

DOI: 10.1002/nme